Available online at www.sciencedirect.com
ScienceDirect
Journal of Computational Physics 218 (2006) 417–428
JOURNAL OF COMPUTATIONAL PHYSICS
www.elsevier.com/locate/jcp

Numerical simulations of jet pinching-off and drop formation using an energetic variational phase-field method

Xiaofeng Yang [a], James J. Feng [b], Chun Liu [c], Jie Shen [a,*]

[a] Department of Mathematics, Purdue University, West Lafayette, IN 47907, United States
[b] Departments of Mathematics and Chemical and Biological Engineering, University of British Columbia, Vancouver, BC, Canada V6T 1Z2
[c] Department of Mathematics, Pennsylvania State University, University Park, PA 16802, United States

Received 10 August 2005; received in revised form 27 January 2006; accepted 20 February 2006
Available online 19 April 2006

Abstract

We study the retraction and pinch-off of a liquid filament and the formation of drops by using an energetic variational phase field model, which describes the motion of mixtures of two incompressible fluids. An efficient and accurate numerical scheme is presented and implemented for the coupled nonlinear systems of Navier–Stokes type linear momentum equations and volume preserving Allen–Cahn type phase equations. Detailed numerical simulations for a Newtonian fluid filament falling into another ambient Newtonian fluid are carried out. The dynamical scaling behavior and the pinch-off behavior, as well as the formation of the consequent satellite droplets are investigated.
© 2006 Elsevier Inc. All rights reserved.

Keywords: Drop formation; Pintching; Two phase flow; Phase-field method; Spectral method; Incompressible flow

1. Introduction

There are growing scientific interests in the dynamics of drop formation from a capillary tube because of applications in many areas such as atomization, inkjet printing, separation process and dynamic surface tension measurement. As a drop falls under gravitational force into an ambient fluid (such as air or another liquid), it remains connected with its source for some time by a long straight liquid filament. The filament then pinches off and satellite droplets may form. The different spatial and temporal scales of this complex process reflect the specific physical and rheological properties of the filament and those of the ambient material.

Although filament breakup/pinching-off and drop formation have been studied for more than a century, there are still many unresolved issues due to its complexity. Most of the experimental work was primarily focused on determining the number of satellites drops, and was not particularly concerned with the dynamics

* Corresponding author. Tel.: +1 765 494 1923; fax: +1 928 223 3244.
E-mail addresses: xfyang@math.purdue.edu (X. Yang), jfeng@math.ubc.ca (J.J. Feng), liu@math.psu.edu (C. Liu), shen@math.purdue.edu (J. Shen).

0021-9991/$ - see front matter © 2006 Elsevier Inc. All rights reserved.
doi:10.1016/j.jcp.2006.02.021

of individual satellite drops [13]. Zhang and Basaran [38] used high-speed visualization to study the effects of physical properties, flow rate, tube radius, tube wall thickness, etc., on the primary drop volume and the fate of satellite drops of glycerol/water solutions forming from the capillary tube. Henderson, et al. [14] used highly viscous liquids to study the pinch-off of primary drops from the main thread and the pinch-off of the main thread from the fluid in the capillary tube. Robinson and Steen [24] and Chen et al. [5] observed that a fluid interface can overturn prior to pinch-off even in the presence of moderate viscosity. There have been numerous theoretical and numerical studies as well. Schulkes [25] used the boundary element method (BEM) to solve for the potential flow inside a growing drop to predict the dynamics of drop formation. Wilkes et al. [32] studied the formation and pinch-off of Newtonian liquid drops from a tube using an axisymmetric algorithm based on a Galerkin finite element method (G/FEM). Zhang [37] used the volume-of-fluid (VOF) method to predict the formation of a series of liquid drops in air. However, as pointed out in [21], this study, along with that of Gueyffier et al. [12], did not capture the fine details in experimental observations since the drop shape prior to breakup and the subsequent satellite dynamics were not adequately resolved. More recently, Notz and Basaran [21] used a moving finite element method with an elliptic mesh-generation scheme to study the dynamics of contracting filaments at different Ohnesorge numbers. They showed that as the Ohnesorge number increases, the shape of the breaking drop changes dramatically, and a series of secondary filament breaking may take place.

All of the aforementioned simulations treated the problem as a free-surface problem governed by the interactions between bulk properties of the filament fluid and ambient fluid, the surface tension and the gravitational force. The interface represents a jump in properties such as density and viscosity, and its position evolves in time with the fluid velocity field – the kinematic condition. We take a fundamentally different approach in this paper. The interface will be viewed as a transition layer where the two fluids mix to a certain degree. The mixing is determined by molecular interactions between the two species, and can be described by a stored "mixing energy", which represents the balance between the competing phobic/philic relation between the filament material and the ambient fluid. In this phase-field framework, the overall hydrodynamics of the system will be the result of competition between the kinetic energy and this elastic mixing energy. Through the transport of a phase-field variable ϕ, the elastic energy will be responsible for the appearance of the induced elastic stress in the momentum equation, by the Least Action Principle. This idea dates back to the work of Lord Rayleigh and van der Waals in the 19th century (see the survey paper by Anderson et al. [1]). Based on an energetic variational formulation, Liu and Shen [18] employed a phase field model to describe the mixture of two incompressible Newtonian fluids. The "mixing energy" studied there is related to the usual Ginzburg–Landau model for phase evolutions. The strengths and limitations of this type of models have been summarized by Feng et al. [10] Recently, such a method has been applied to study mixtures of more complex materials, such as viscoelastic fluids and liquid crystals, together with other surface properties, such as the Marangoni effects [34,35,19]. Such approaches have also been employed by many other people, see for examples [18,33,16,2,27,17].

In this paper, we use such an energetic variational phase-field model to simulate the pinch-off and drop formation phenomena in axisymmetric geometries. As demonstrated in the earlier works [18,33,16,2,27], the phase-field method enjoys the advantages of admitting topological changes and allowing more complex material properties such as non-Newtonian rheology, bulk elastic properties and different surface effects. In this paper, we choose to use an Allen–Cahn type of phase equation with a Lagrangian multiplier to preserve the overall mass of filaments and drops. This choice represents a special regularization of the kinematic condition for the free interface in the classical sharp-interface approach. The coupled nonlinear system is then solved by using a stiffly stable spectral-projection method [20] which was also used in our previous studies [9,18,33].

The rest of the paper is organized as follows. In the next section, we will first describe our phase field model. In Section 3, we shall present our numerical method for the coupled nonlinear evolution system in an axisymmetric geometry. We will employ several techniques which are particularly suitable for the problem at hand. The resultant numerical scheme is stiffly stable, mass conservative, highly efficient and capable of handling variable density and viscosity. In Section 4, we present numerical results for the simulation of several scenarios of pinch-off and drop formations. Some concluding remarks are given in the last section.

2. A phase field model for the mixture of two incompressible fluids

Let Ω be a domain filled with two incompressible fluids separated by a free moving interface. In this study, one fluid is a filament or drop while the other is the ambient fluid. As in [18], we introduce a phase function $\phi(x)$, defined on the physical domain Ω, to label the inside and the outside of the filament/drop. Then, the level set $\{x : \phi(x) = 0\}$ represents the interface, while $\{x : \phi(x) > 0\}$ represents the inside of the interface and $\{x : \phi(x) < 0\}$ the outside. Since this function is defined on the Eulerian reference coordinates, we do not need to follow the motion of the specific level set; instead we derive the corresponding interface motion through the dynamics of this phase function ϕ. In fact, the phase-field methods, as well as the level set methods [22,28], the volume of fluid (VOF) methods [23] and the lattice Boltzmann method [31,6,7,36], represent geometric changes, which are naturally parametrized in the Lagrangian (reference) coordinates, in the Eulerian (observer) framework.

We will established a phase field formulation based on an energetic variational approach [18,33]. As for the interaction between the fluids, we introduce the following elastic "mixing energy":

$$W(\phi, \nabla\phi) = \int_\Omega \left[\frac{1}{2}|\nabla\phi|^2 + \frac{1}{4\eta^2}(\phi^2 - 1)^2\right] \mathrm{d}x. \tag{1}$$

The first part of the energy represents the hydrophilic interaction between the molecules and the second part the hydrophobic interactions. It is the competition between these two parts of the energy that gives the hydrostatic configuration of the interface (see, for instance, [18]). The constant η can be viewed as the ratio between these two parts of energies.

With the above energy, it can be shown that the interface is represented by $\{x : \phi(x, t) = 0\}$ with a transition layer of thickness η. The classical sharp interface models will coincide with this approach away from the interface (η can be viewed as a physical transitional region or simply the resolution parameter). The pure kinematic condition of the sharp interface can be translated into:

$$\phi_t + \boldsymbol{u} \cdot \nabla\phi = 0, \tag{2}$$

where $\boldsymbol{u}$ is the fluid velocity. This represents the transport of the phase function along the interface. It is another representation of the immiscibility of the two fluids. In this case, ϕ can also be viewed as the volume fraction (after an linear transformation), or even the density. On the other hand, the dynamics of ϕ in a phase-field (or diffuse-interface) approach can be relaxed (approximated) according to either Allen–Cahn or Cahn–Hillard types of gradient flow, depending on the choice of different dissipative mechanisms. In this paper, we choose to use the Allen–Cahn dynamics since its numerical treatment is simpler than that of the Cahn–Hilliard type which involves fourth-order differential operators. For both Allen–Cahn and Cahn–Hilliard dynamics, it can be shown that transition profile is maintained through the dynamics and the transitional width will not increase in time (cf. [10]). This is a key factor for the validity of the phase-field method. In fact, both Allen–Cahn and Cahn–Hilliard dynamics can be viewed as energetic variation based approximations of the transport equation of ϕ (2) in such a way that the transition layer does not spread into the domain.

Even though the transport equation (2) is relaxed in a phase-field model, in many applications, it is still desirable that the integral of ϕ – the volume fractions of the two immiscible fluids in the sharp-interface limit – is conserved. It is well-known that the Cahn–Hilliard type dynamics conserves the volume fractions while the Allen–Cahn type dynamics does not. Hence, we introduce a Lagrange multiplier $\xi(t)$ into the Allen–Cahn model to conserve the volume. More precisely, let $F(\phi) = \frac{1}{4\eta^2}(\phi^2 - 1)^2$ be the usual double-well potential and $f(\phi) = F'(\phi)$, the modified (fluid transported) Allen–Cahn phase equation reads:

$$\begin{aligned} &\phi_t + \boldsymbol{u} \cdot \nabla\phi = -\gamma \frac{\delta W}{\delta \phi} = \gamma(\Delta\phi - f(\phi) + \xi(t)), \\ &\frac{\mathrm{d}}{\mathrm{d}t}\int_\Omega \phi \,\mathrm{d}x = 0, \end{aligned} \tag{3}$$

where $\xi(t)$ is the Lagrange multiplier corresponding to the constant volume constraint in the last equation. The parameter γ represents the elastic relaxation time. Again, we want to point out that the dynamics of ϕ represents an approximation of the original kinematic condition on the interface. We are not interested in

the validity of the phenomena they represent. This is in contrast to the vast existing work on the related models for the presence of special dynamics [15,3,4]. It can be regarded as an smoothing at the level of the modelling, instead of the conventional numerical smoothing such as the upwind scheme, which introduces an artificial diffusion in the simulations. We can see that when $\gamma \to 0$, we recover the transport equation for ϕ (2), as the interface moves with the flow, we recover the kinematic boundary condition in the sharp interface model. Finally, we notice that the volume preservation constraint we introduced above is a global preserving constraint, instead of the physical local constraint. Again, the purpose here is just for the numerical/modeling approximation. In the limit of γ approaching zero, such discrepancy will disappear.

We now describe the governing equations for the fluid flow. The momentum equation takes the form, which can be derived by the least action principle [18,33]:

$$\rho(\boldsymbol{u}_t + (\boldsymbol{u}\cdot\nabla)\boldsymbol{u}) = -\nabla p + \nabla\cdot\sigma, \tag{4}$$

where ρ is the density, $\boldsymbol{u}$ is the velocity, p is the pressure and σ is the deviatoric stress tensor which includes the viscous tensor and the induced elastic stress tensor. When we take into account the competition between the kinetic energy and the elastic energy (i.e., the mixing energy), we find:

$$\sigma = \mu[\nabla\boldsymbol{u} + (\nabla\boldsymbol{u})^t] - \lambda(\nabla\phi\otimes\nabla\phi), \tag{5}$$

where μ is the dynamic viscosity coefficient, and the term $\nabla\phi\otimes\nabla\phi$ is the induced elastic stress due to mixing energy, and λ corresponds to the ratio between the kinetic energy and the elastic energy. In this application, it is related to the surface tension coefficients.

The final hydrodynamical coupled system will have the following energy identity:

$$\frac{\mathrm{d}}{\mathrm{d}t}\int \frac{1}{2}\rho|\boldsymbol{u}|^2 + \lambda W(\phi)\,\mathrm{d}x = -\int \nu|\nabla\boldsymbol{u}|^2 + \frac{\lambda}{\gamma}|\phi_t + \boldsymbol{u}\cdot\nabla\phi|^2\,\mathrm{d}x. \tag{6}$$

When the two fluids have different viscosities ρ_1 and ρ_2, (assuming that the difference between the two densities ρ_1 and ρ_2 is relatively small), we shall incorporate the classical Boussinesq approximation into the momentum equation (4):

$$\rho_0(\boldsymbol{u}_t + (\boldsymbol{u}\cdot\nabla)\boldsymbol{u}) = -\nabla p + \nabla\cdot\sigma + \boldsymbol{f}, \tag{7}$$

where $\rho_0 = (\rho_1+\rho_2)/2$ and the difference between the actual density ρ and ρ_0 is modeled by a buoyancy force

$$\boldsymbol{f} = -[(1+\phi)(\rho_1-\rho_0) + (1-\phi)(\rho_2-\rho_0)]\boldsymbol{g}_0, \tag{8}$$

where $\boldsymbol{g}_0$ is the gravity force.

Setting $\rho_0 = 1$ for the sake of simplicity and writing $\nu = \mu/\rho_0$, the system governing the mixture of two incompressible fluids can be written as follows:

$$\begin{aligned} &\boldsymbol{u}_t + (\boldsymbol{u}\cdot\nabla)\boldsymbol{u} + \nabla p - \nabla\cdot[\nu(\nabla\boldsymbol{u} + (\nabla\boldsymbol{u})^t)] + \lambda\nabla\cdot(\nabla\phi\otimes\nabla\phi) = \boldsymbol{f},\\ &\nabla\cdot\boldsymbol{u} = 0, \end{aligned} \tag{9}$$

and

$$\begin{aligned} &\phi_t + (\boldsymbol{u}\cdot\nabla)\phi = \gamma(\Delta\phi - f(\phi) + \xi(t)),\\ &\frac{\mathrm{d}}{\mathrm{d}t}\int_\Omega \phi\,\mathrm{d}x = 0. \end{aligned} \tag{10}$$

The coupled nonlinear system (9) and (10) is supplemented with the initial conditions

$$\boldsymbol{u}|_{t=0} = u_0, \quad \phi|_{t=0} = \phi_0 \tag{11}$$

and appropriate boundary conditions for $\boldsymbol{u}$ and ϕ to be specified below.

3. Filament breakup and drop formation in a cylinder: setup of the problem

We are interested in the dynamics of a filament breakup and a falling drop along the axis of a cylinder filled with an ambient fluid. Assuming that the flow is axisymmetric, we can rewrite the system using the cylindrical

coordinates (r, z) in the two-dimensional axisymmetric domain $D = \{(r,z) : 0 < r < R, 0 < z < H\}$. For simplicity, we shall assume for the moment that the two fluids have the same viscosity. The case of different viscosities will be addressed at the end of this section.

Let $\boldsymbol{u} = (u, v, w)^t$, where u, v, w are, respectively, the velocity components in the axial (r), azimuthal (θ) and vertical (z) directions. We denote by

$$\widetilde{\nabla} = (\partial_r, 0, \partial_z)^t, \quad \widetilde{\nabla}^2 = \partial_r^2 + \frac{1}{r}\partial_r + \partial_z^2, \tag{12}$$

the gradient and Laplace operators in the cylindrical coordinates, respectively. The divergence operator in the cylindrical coordinates is

$$\widetilde{\nabla} \cdot \boldsymbol{u} := \frac{1}{r}(ru)_r + w_z. \tag{13}$$

Let $[\boldsymbol{f}]_r$ and $[\boldsymbol{f}]_z$ denote the component of $\boldsymbol{f}$ in the r and z direction. Then, the coupled nonlinear system (9) and (10) in the axisymmetric cylindrical coordinates reads

$$\begin{aligned}
&u_t + uu_r + wu_z - \frac{1}{r}v^2 = -p_r + \nu\left(\widetilde{\nabla}^2 u - \frac{1}{r^2}u\right) - \lambda[\widetilde{\nabla} \cdot (\widetilde{\nabla}\phi \otimes \widetilde{\nabla}\phi)]_r,\\
&v_t + uv_r + wv_z + \frac{1}{r}uv = \nu\left(\widetilde{\nabla}^2 v - \frac{1}{r^2}v\right),\\
&w_t + uw_r + ww_z = -p_z + \nu\widetilde{\nabla}^2 w - \lambda[\widetilde{\nabla} \cdot (\widetilde{\nabla}\phi \otimes \widetilde{\nabla}\phi)]_z,\\
&\widetilde{\nabla} \cdot \boldsymbol{u} := \frac{1}{r}(ru)_r + w_z = 0
\end{aligned} \tag{14}$$

and

$$\begin{aligned}
&\phi_t + u\phi_r + w\phi_z = \gamma(\widetilde{\nabla}^2\phi - f(\phi) + \xi),\\
&\frac{\mathrm{d}}{\mathrm{d}t}\int_D r\phi \,\mathrm{d}r\,\mathrm{d}z = 0.
\end{aligned} \tag{15}$$

Since the enclosed cylinder is filled with fluids, the boundary conditions for u are [20]:

$$u|_{\partial D} = v|_{\partial D} = 0, \quad w|_{\partial D\setminus\Gamma_1} = 0, \quad \frac{\partial w}{\partial n}|_{\Gamma_1} = 0, \tag{16}$$

where $\Gamma_1 = \{(r,z): r = 0, 0 < z < H\}$, n is the outward normal. The boundary condition for ϕ is

$$\left.\frac{\partial\phi}{\partial n}\right|_{\partial D\setminus\Gamma_1} = 0. \tag{17}$$

We now describe our numerical approach. The time discretization is based on a semi-implicit second-order rotational pressure-correction scheme for (14) (cf. [11]) and a stabilized semi-implicit scheme for (15). To simplify the presentation, we use

$$\tilde{\Delta} = \begin{pmatrix} \widetilde{\nabla}^2 - \frac{1}{r^2} & & \\ & \widetilde{\nabla}^2 - \frac{1}{r^2} & \\ & & \widetilde{\nabla}^2 \end{pmatrix}$$

to denote the vector Laplace operator in cylindrical coordinates, and set

$$\begin{aligned}
&\boldsymbol{N}_1(\boldsymbol{u}) = \left(uu_r + wu_z - \frac{1}{r}v^2, uv_r + wv_z + \frac{1}{r}uv, uw_r + ww_z\right)^t,\\
&\boldsymbol{N}_2(\phi) = \widetilde{\nabla} \cdot ((\phi_r, 0, \phi_z) \otimes (\phi_r, 0, \phi_z))^t,\\
&N_3(\boldsymbol{u}, \phi) = (\boldsymbol{u} \cdot \widetilde{\nabla})\phi.
\end{aligned}$$

Assuming $(\boldsymbol{u}^k, p^k, \phi^k)$ and $(\boldsymbol{u}^{k-1}, p^{k-1}, \phi^{k-1})$ are known, we first solve $(\tilde{\boldsymbol{u}}^k, \boldsymbol{u}^k, p^k)$ from a semi-implicit rotational pressure-correction method (see, for instance, [11]) for (14):

$$\begin{cases} \frac{3\tilde{\boldsymbol{u}}^{k+1}-4\boldsymbol{u}^k+\boldsymbol{u}^{k-1}}{2\delta t} - \nu\tilde{\Delta}\tilde{\boldsymbol{u}}^{k+1} + \tilde{\nabla}p^k = -(2\boldsymbol{N}_1(\boldsymbol{u}^k) - \boldsymbol{N}_1(\boldsymbol{u}^{k-1})) + (2\boldsymbol{N}_2(\boldsymbol{\phi}^k) - \boldsymbol{N}_2(\boldsymbol{\phi}^{k-1})) \\ (\tilde{u}^{k+1}, \tilde{v}^{k+1})|_{\partial D} = 0, \quad \tilde{w}^{k+1}|_{\partial D\setminus\Gamma_1} = 0, \quad \frac{\partial\tilde{w}^{k+1}}{\partial n}|_{\Gamma_1} = 0; \end{cases} \tag{18}$$

$$\begin{cases} -\tilde{\nabla}^2\psi^{k+1} = \frac{1}{2\delta t}\tilde{\nabla}\cdot\tilde{\boldsymbol{u}}^{k+1}, \\ \left.\frac{\partial\psi^{k+1}}{\partial n}\right|_{\partial D} = 0; \end{cases} \tag{19}$$

and

$$\begin{aligned} p^{k+1} &= p^k + \psi^{k+1} - \nu\tilde{\nabla}\cdot\tilde{\boldsymbol{u}}^{k+1}, \\ \boldsymbol{u}^{k+1} &= \tilde{\boldsymbol{u}}^{k+1} - \frac{2\delta t}{3}\tilde{\nabla}\psi^{k+1}. \end{aligned} \tag{20}$$

Then, we update ϕ^{k+1} by using the stabilized semi-implicit second-order scheme for (15):

$$\begin{cases} \frac{3\phi^{k+1}-4\phi^k+\phi^{k-1}}{2\delta t} - \gamma\tilde{\nabla}^2\phi^{k+1} = -\gamma\left(2f(\phi^k) - f(\phi^{k-1}) + \frac{s}{\eta^2}(\phi^{k+1} - 2\phi^k + \phi^{k-1})\right) \\ \qquad\qquad -(2N_3(\boldsymbol{u}^{k+1}, \phi^k) - N_3(\boldsymbol{u}^{k+1}, \phi^{k-1})) + \gamma\xi^{k+1}, \\ \int_D r\phi^{k+1}\,\mathrm{d}r\,\mathrm{d}z = \int_D r\phi^k\,\mathrm{d}r\,\mathrm{d}z, \\ \left.\frac{\partial\phi^{k+1}}{\partial\vec{n}}\right|_{\partial D\setminus\Gamma_1} = 0. \end{cases} \tag{21}$$

Several remarks are in order:

- One can initialize $(\boldsymbol{u}^1, p^1, \phi^1)$ by using a first-order version of (18)–(21).
- We derive easily from (21) that

$$\xi^{k+1} = \frac{1}{|D|}\int_D r(2f(\phi^k) - f(\phi^{k-1}))\,\mathrm{d}r\,\mathrm{d}z. \tag{22}$$

  Hence, the Lagrange multiplier ξ^{k+1} can be computed directly from previous data.
- We recall that $f(\phi) = \frac{1}{\eta^2}(1-|\phi|^2)\phi$ so the explicit treatment of this term usually lead to a severe restriction on the size of time step δt when $\eta \ll 1$. We introduced in (21) an extra dissipative term $\frac{s}{\eta^2}(\phi^{k+1} - 2\phi^k + \phi^{k-1})$, which is of order $\frac{s\delta t^2}{\eta^2}$, to improve the stability while preserving the simplicity. The parameter s is proportional to the amount of artificial dissipation added in the numerical scheme. Larger s will lead to a more stable but less accurate scheme. In our numerical simulations, we used $s = 5$ which appeared to provide a good balance between stability and accuracy.
- At each time step, one only needs to solve a sequence of Poisson-type equations. This is to be accomplished by using the Legendre–Galerkin method (cf. [20,29,30]).
- The scheme can be easily generalized to allow different viscosities ν_1 and ν_2 for the two fluids. In this case, we can use the following harmonic "averaged" viscosity (through ϕ) as the mixture viscosity:

$$\frac{1}{\nu(\phi)} = \frac{1+\phi}{2\nu_1} + \frac{1-\phi}{2\nu_2}. \tag{23}$$

  Then, the new viscous term $\tilde{\nabla}\cdot(\nu(\phi)(\tilde{\nabla}\boldsymbol{u} + (\tilde{\nabla}\boldsymbol{u})^t))$ at $t_{k+1} = (k+1)\delta t$ can be approximated to a second-order accuracy by replacing the term $-\nu\tilde{\Delta}\tilde{\boldsymbol{u}}^{k+1}$ in (14) with

$$-\hat{\nu}\tilde{\Delta}\tilde{\boldsymbol{u}}^{k+1} - 2\tilde{\nabla}\cdot\left((\nu(\phi^k) - \hat{\nu})(\tilde{\nabla}\boldsymbol{u}^k + (\tilde{\nabla}\boldsymbol{u}^k)^t)\right) + \tilde{\nabla}\cdot\left((\nu(\phi^{k-1}) - \hat{\nu})(\tilde{\nabla}\boldsymbol{u}^{k-1} + (\tilde{\nabla}\boldsymbol{u}^{k-1})^t)\right), \tag{24}$$

  where $\hat{\nu}$ is the harmonic average determined by $\frac{1}{\hat{\nu}} = \frac{1}{2\nu_1} + \frac{1}{2\nu_2}$. Hence, the solution procedure in the variable viscosity case is essentially the same as in the constant viscosity case.

4. Numerical simulations

In this section, we describe our numerical simulations using the numerical method described in the previous section. We shall simulate two processes: the retraction of a fluid filament and the fall and detachment of a drop in an ambient fluid. The driving force is surface tension in the former and the gravity in the latter. We will examine in particular how the viscosity of the fluids affects the pinch-off of the filament and formation of satellite droplets.

In all the numerical examples presented below, we used the following parameters:

$$\gamma = 0.02, \quad \lambda = 0.01, \quad \eta = 0.02. \tag{25}$$

Other parameters are specified below and in the figure captions. We use N and M to denote the numbers of Legendre polynomials used in the z and r directions, respectively.

4.1. Shape evolution and breakup of retracting filaments

In this set of numerical simulations, we consider the retraction of a cylindrical filament of radius $R = \frac{1}{4}$ and height $H = 5.5$ placed at the axis of a cylinder of radius $R = 1$ and height $H = 6$ filled with another ambient fluid (see the first plot in Fig. 1).

We consider first the case where the two fluids have the same density and same viscosity, and we examine the effect of varying the viscosity v on the formation of satellite drops. Initially, we set $\phi = 1$ inside the filament and $\phi = -1$ in the ambient fluid.

Note that the results will depend on the combined effects of the surface tension, the viscosity and the elastic relaxation time. When the last effect is absent (or very small), the dominant time scale of the problem will be the capillary time (cf. [33]) which can be represented by the ratio of the kinematic viscosity v and the interfacial tension coefficient λ. Within a certain range, as viscosity decreases, the Allen–Cahn dynamic will evolve faster. However, as the viscosity decreases beyond this range, the elastic relaxation effect will be more and more dominant and more complicated phenomena will occur.

- We start with a relatively high viscosity $v = 1$, the filament contracts and slowly forms a single droplet; see Fig. 1.
- Then, we set $v = 0.02$. Relative to the lower viscosity, the surface tension is larger in this case, and the filament develops bulbous ends shortly after it starts to contract ($t = 1$). Eventually, capillary instability develops and breaks the filament into two drops, see Fig. 2. Note that the topological changes are handled seamlessly with the phase-field model.
- The result for $v = 0.005$ is shown in Fig. 3. Here, the filament also forms bulbous ends followed by capillary instability in the middle. Unlike in Fig. 2, the filament fails to pinch-off despite the appearance of a very thin neck at $t = 2.6$. Instead, the neck thickens subsequently and produces a single drop. The drop undergoes damped oscillations in shape and will eventually become spherical. The failure for pinch-off in this case may be due to the elastic relaxation mechanism in the Allen–Cahn equation for ϕ. It appears that the

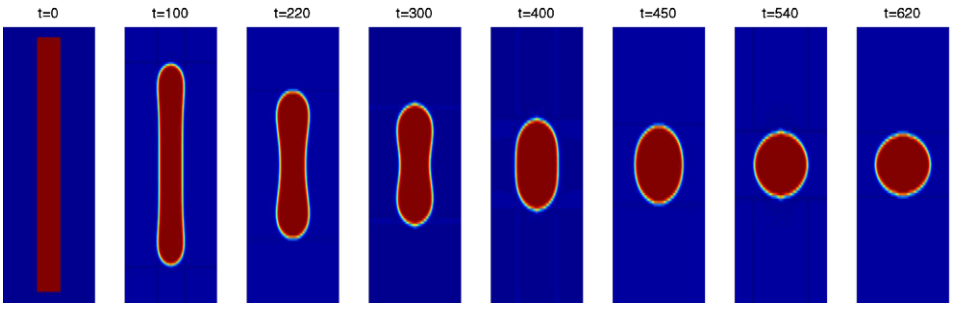

Fig. 1. Snapshots of the interface with $v = 1$ and $g = 0$. Numerical parameters: $N = 160$, $M = 88$, $\delta t = 0.1$, $s = 5$.

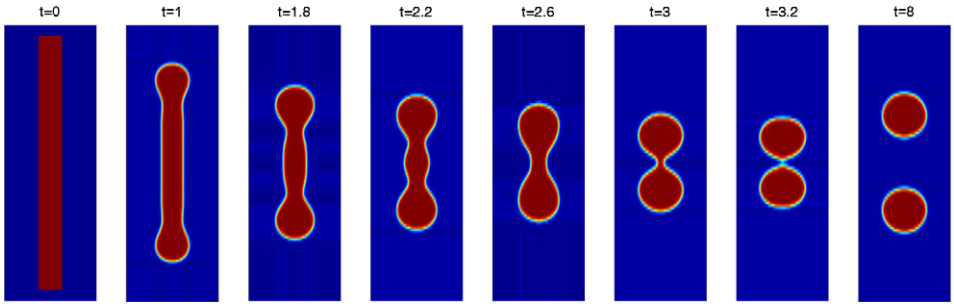

Fig. 2. Snapshots of the interface with $v = 0.02$ and $g = 0$. Numerical parameters: $N = 160$, $M = 88$, $\delta t = 0.002$, $s = 5$.

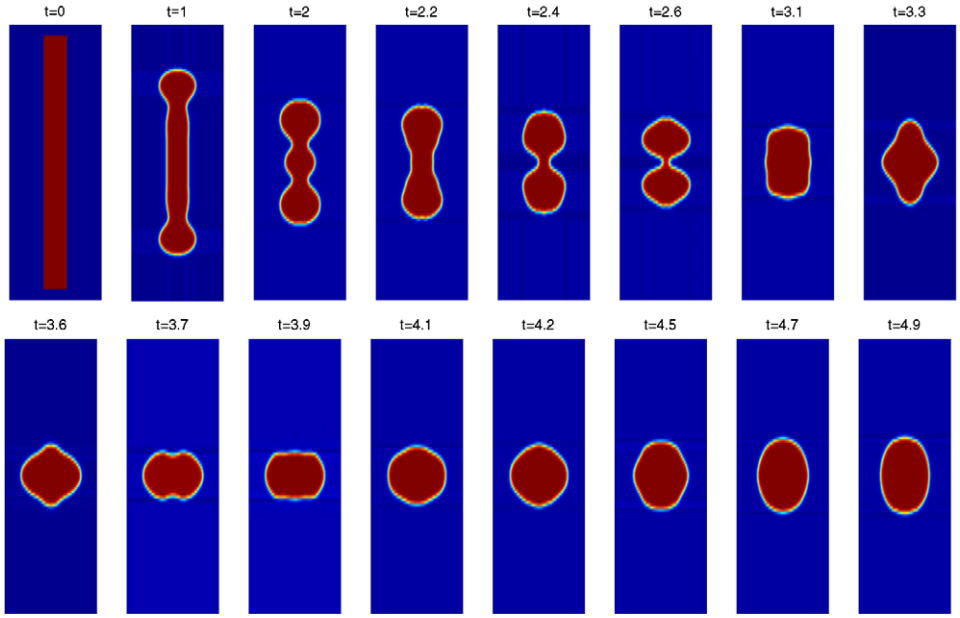

Fig. 3. Snapshots of the interface with $v = 0.005$ and $g = 0$. Numerical parameters: $N = 160$, $M = 88$, $\delta t = 0.0005$, $s = 5$.

interfacial diffusion due to the Allen–Cahn dynamics interferes before the pinch-off mechanism has time to take effect. In fact, if we decrease the elastic relaxation coefficient γ to $\gamma = 0.002$, the filament will eventually pitch off. We refer to Section 5.2 in [10] for a more elaborate discussion in this regard.

- Fig. 4 shows the interfacial evolution with $v = 0.002$. Here, the behavior of the filament changes in a surprising fashion. Initially, bulbous ends form on the contracting filament while capillary instability quickly grows on the straight section of the filament, with a shorter wavelength than in the more viscous cases. It looks as if the filament will break up and form four satellite drops (see the plot at $t = 1.4$). However, the undulation in the middle soon dies out and gives way to a three-bulb shape at $t = 1.85$. It eventually pinches off into three satellite drops.
- Fig. 5 shows a run with the smallest viscosity tested, $v = 0.001$. For $t \leqslant 1.4$, the evolution is similar to the case $v = 0.002$. However, for $t > 1.4$, their behaviors differ somewhat. In fact, the middle part does not contract as in Fig. 4; the capillary force dominates the viscous force and causes the bulbous ends to pinch off at a much earlier time ($t = 1.475$).

In conclusion, we can see that pinch-off is the result of complicated competition among various effects. If the viscosity is too large, pinch-off will not occur because the capillary instability develops slowly, and does not have time to take effect before the filament retracts. If the viscosity is too small, the filament may also fail to

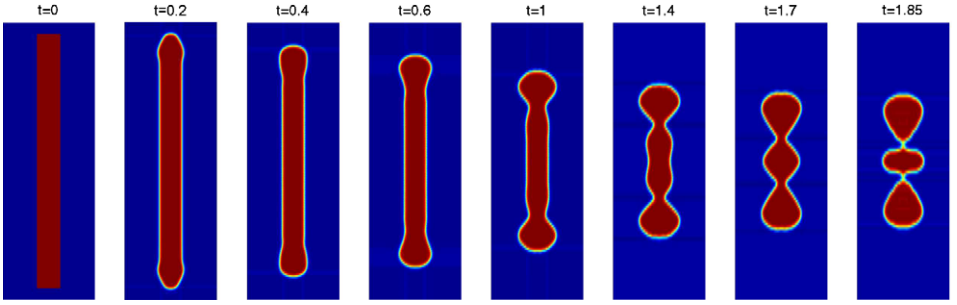

Fig. 4. Snapshots of the interface with $v = 0.002$ and $g = 0$. Numerical parameters: $N = 160$, $M = 88$, $\delta t = 0.0002$, $s = 5$.

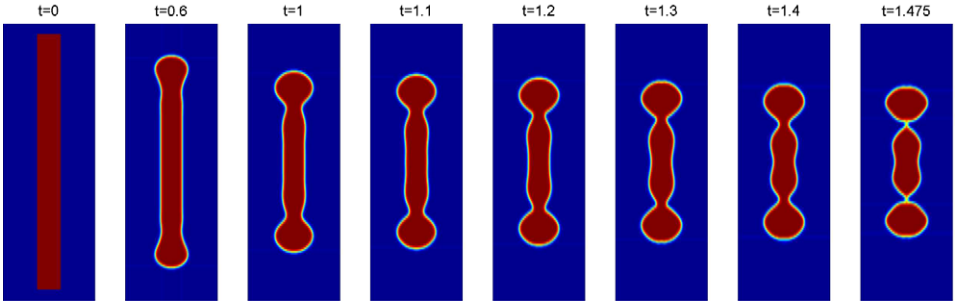

Fig. 5. Snapshots of the interface with $v = 0.001$ and $g = 0$. Numerical parameters: $N = 200$, $M = 100$, $\delta t = 0.00005$, $s = 5$.

pinch off as the elastic relaxation will interfere with the pinch-off mechanism. The tradeoff between numerical accuracy and interfacial integrity has been discussed by Jacqmin [16].

Let L_0 be the dimensionless initial aspect ratio between half of the filament height and its radius, i.e., $L_0 = \frac{5.5/2}{1/4} = 11$ in Figs. 1–6. As found in other studies (see [26,21]), there is a critical number $L_{0,c}$, dependent on the interfacial tension and viscosity, such that the filament does not break for $L_0 < L_{0,c}$. Notz and Basaran [21] examined the dependence of $L_{0,c}$ on the Ohnesorge number $Oh = \frac{\mu}{\sqrt{\rho R \sigma}}$, where μ is the dynamical viscosity, σ is the interfacial tension and R is the radius of the filament. They observed that $L_{0,c}$ increases with Oh (see Table 3 in [21]). In our results, the kinematic viscosity v plays the role of the Ohnesorge number so we have also numerically determined $L_{0,c}$ in terms of v and listed the results in Table 1. For example, the initial filament with $L_0 \geqslant 13 \pm 0.25$ will break up when $v = 10^{-2}$, but when $v = 2 \times 10^{-3}$, $L_0 \geqslant 9$ is needed for the breakup to occur. This appears to be qualitatively consistent with the results in [21]. Note that in [21], the ambient fluid is the air, while in our study the ambient fluid is a different fluid with the same density and viscosity as the filament. So the two results can only be compared qualitatively.

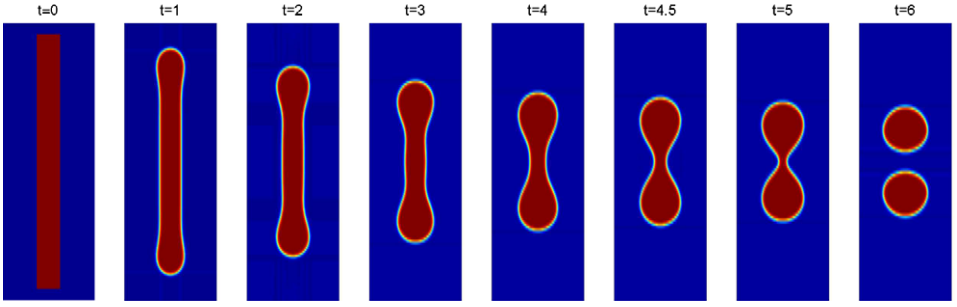

Fig. 6. Snapshots of the interface with different viscosities: $v_1 = 0.02$, $v_2 = 0.07$ and $g = 0$. Numerical parameters: $N = 160$, $M = 88$, $\delta t = 0.005$, $s = 5$.

Table 1
Effect of viscosity on the critical initial aspect ratio $L_{0,c}$ below which a filament does not break

v	10^{-3}	2×10^{-3}	4×10^{-3}	6×10^{-3}	8×10^{-3}	10^{-2}
$L_{0,c}$	7 ± 0.25	9 ± 0.25	11 ± 0.25	12 ± 0.25	12.5 ± 0.25	13 ± 0.25

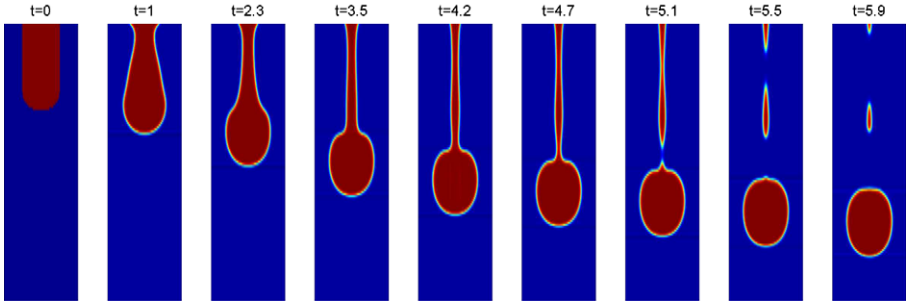

Fig. 7. Snapshots of the interface with $v=1$, $\rho_1=\frac{3}{2}$, $\rho_2=\frac{1}{2}$ and $g=-12$ in (8). Numerical parameters: $N=160$, $M=88$, $\delta t=0.01$, $s=5$.

As the last example in this subsection, we consider a case where the two fluids have the same density but different viscosities. More precisely, we set $v_1=0.02$ inside the filament and $v_2=0.07$ outside. The result is shown in Fig. 6. Here, the situation is very similar to the case in Fig. 2 where the fluids have the same viscosity $v=0.02$. The filament contracts and pinch-off into two satellites at a slightly early time.

4.2. The dynamics of dripping

When a drop falls from a faucet, it remains attached to the source by an elongating liquid filament until the filament pinches off. A similar process occurs during the inkjet printing process. Since currently it is numerically difficult to handle the very large density ratio between fluids such as water and air, we shall simulate this dripping process by using the Boussinesq approximation (4)–(8) which is only valid for small density difference, to represent the gravitational force due to a density difference between the jet and the ambient fluid. We set the initial interface shape to be a spherical cap as shown in the first plot of Fig. 7. The height and the radius of the cylinder is set to be 7.5 and 1, respectively. The boundary conditions for $\boldsymbol{u}$ and ϕ are still given by (16) and (17), with zero velocity at the mouth of the "faucet".

The full process of the falling drop is shown in Fig. 7. As the liquid filament is stretched by gravity, a neck forms near its base which elongates and becomes thinner. In the meantime, the lower end of the filament turns into a round drop under capillary forces (see the plots at $t=2.3$ in Fig. 7). The falling drop continues to stretch the thread, and eventually the Rayleigh instability leads to the pinch-off of the main drop at $t=5.1$. A secondary pinch-off takes place at $t=5.5$, and produces a small satellite drop. Note that the hanging jets seem to have shrunk somewhat from $t=5.5$ to $t=5.9$. This is not a failure of mass conservation since only the total mass, not the mass of each individual part, is conserved. Rather it is an effect of the Allen–Cahn dynamics and could be controlled by taking a smaller relaxation coefficient γ in the Allen–Cahn equation.

5. Concluding remarks

We presented an energetic variational phase-field method for simulating interfacial dynamics in filament breakup and drop formation. The phase-field approach avoids the need for interface tracking and can easily accommodate topological changes such as pinch-off. A stabilized semi-implicit second-order time-marching scheme coupled with Legendre–Galerkin spectral discretization has proved to be efficient and accurate for this class of problems. As numerical examples, we simulated the retraction and breakup of a fluid filament in

another ambient fluid and the fall and pinch-off of drops from a pendant drop under gravity. The results are consistent with prior computations and experiments.

As we have indicated in this paper (as in all the previous works in the area), the phase-field method is a very versatile and robust method for studying interfacial motion in multi-component flows. It casts geometric evolution in Lagrangian coordinates into a Eulerian formulation, and provides a way to represent surface effects as bulk effects. The whole process allows us to use an energetic variational formulation that in turn makes it possible to ensure the stability of corresponding numerical algorithms. The elastic relaxation built into the phase-field dynamics prevents the interfacial mixing layer from spreading out. Moreover, being a physically motivated approximation based on the competition between different parts of the energy functionals, the phase-field model can be adapted easily to incorporate more complex physical phenomena such as Marangoni effect and non-Newtonian rheology [33].

The main challenge of such methods lies in the fact that for real fluid systems, we typically have a good understanding of the bulk but very little information about the interfacial layer. While the properties of the flow away from the interface are independent of the choice of the mixing energy functionals, at least in the limit of $\eta \to 0$, there are applications where the interfacial profile is of significance. Accurate representation of the interface location and the flow at the interface requires high resolution of a thin transitional layer [16]. This is being pursued in ongoing projects that integrate our existing numerical algorithms with adaptive methods (e.g., the moving mesh methods) to better resolve the interface profile. While the Allen–Cahn type approximations have the advantage of keeping the transitional profile and width, it does bring in extra effects due to its own dynamics (such as different coarsening mechanisms).

How to control or avoid such artificial mechanism is also an important research task. Du et al. [8] have made some progress recently in this direction by developing an algorithm to detect and control the topological changes through a generalized Euler number. Finally, more studies are needed to establish accurately the correspondence between the parameters in this model and those from experiments.

Acknowledgements

The research of J. Shen and X. Yang is partially supported in part by NSF-DMS 0456286, NSF-DMS 0509665 and a Purdue Research Foundation PRF-CIRG Grant. The research of C. Liu is partially supported by NSF-DMS 0405850 and NSF-DMS 0509094. J.J. Feng is partially supported by the NSERC, the Canada Research Chair program, and the NNSF of China (No. 20490220). J.J. Feng and C. Liu acknowledge the support of the Petroleum Research Fund of American Chemical Society. The authors thank the Institute of Mathematics and Applications of University of Minnesota for its hospitality and support.

References

[1] D.M. Anderson, G.B. McFadden, A.A. Wheeler, Diffuse-interface methods in fluid mechanics, Appl. Math. Lett. 30 (4) (1998) 139–165.
[2] F. Boyer, A theoretical and numerical model for the study of incompressible mixture flows, Comput. Fluids 31 (2004) 41–68.
[3] A.J. Bray, Theory of phase-ording kinetics, Adv. Phys. 51 (2002) 481–587.
[4] J.W. Cahn, J.E. Hillard, Free energy of a nonuniform system. I. International free energy, J. Chem. Phys. 28 (1958) 258–267.
[5] A.U. Chen, P.K. Notz, O.A. Basaran, Computational and experimental analysis of pinch-off and scaling, Phys. Rev. Lett. 88 (2002) 17–4501.
[6] Shiyi Chen, Gary D. Doolen, Lattice Boltzmann method for fluid flows, in: Annual Review of Fluid Mechanics, Annu. Rev. Fluid Mech., vol. 30, Annual Reviews, Palo Alto, CA, 1998, pp. 329–364..
[7] Shiyi Chen, Gary D. Doolen, Xiaoyi He, Xiaobo Nie, Raoyang Zhang, Recent advances in lattice Boltzmann methods, in: Fluid Dynamics at Interfaces (Gainesville, FL, 1998), Cambridge University Press, Cambridge, 1999, pp. 352–363.
[8] Q. Du, C. Liu, X. Wang, Retrieving topological information for phase field models, SIAM J. Appl. Math. 65 (2005) 1913–1923.
[9] Q. Du, J. Shen, B.Y. Guo, Fourier spectral approximation to a dissipative system modeling the flow of liquid crystals, SIAM J. Numer. Anal. 39 (2001) 735–762.
[10] J.J. Feng, C. Liu, J. Shen, P. Yue, A energetic variational formulation with phase field methods for interfacial dynamics of complex fluids: advantages and challenges, in: M.T. Calderer, E.M. Terentjev (Eds.), Modeling of Soft Matter, vol. IMA 141, Springer, New York, 2005, pp. 1–26.
[11] J.L. Guermond, J. Shen, On the error estimates of rotational pressure-correction projection methods, Math. Comput. 73 (2004) 1719–1737.

[12] D. Gueyffier, J. Li, A. Nadim, R. Scardovelli, S. Zaleski, Volume-of-fluid interface tracking with smoothed surface stress methods for three dimensional flows, J. Comput. Phys. 152 (1999) 423–456.
[13] E.A. Hauser, H.E. Edgerton, B.M. Holt, J.T. Cox Jr., The application of high speed motion picture camera to research on the surface tension of liquids, J. Phys. Chem. 40 (1936) 937–988.
[14] D. Henderson, H. Segur, L.B. Smolka, M. Wadati, The motion of a falling liquid filament, Phys. Fluids 12 (2000) 550–565.
[15] P.C. Hohenberg, B.I. Halperin, Theory of dynamic critical phenoma, Rev. Modern Phys. 49 (1977) 435–479.
[16] D. Jacqmin, Calculation of two-phase Navier–Stokes flows using phase-field modeling, J. Comput. Phys. 155 (1999) 96–127.
[17] J.S. Kim, A continuous surface tension force formulation for diffuse-interface models, J. Comput. Phys. 204 (2005) 784–804.
[18] C. Liu, J. Shen, A phase field model for the mixture of two incompressible fluids and its approximation by a Fourier-spectral method, Physica D 179 (2003) 211–228.
[19] C. Liu, J. Shen, J.J. Feng, P. Yue, Variational approach in two-phase flows of complex fluids: transport and induced elastic stress, in: A. Miranville (Ed.), Mathematical Models and Methods in Phase Transitions, Nova Publications, 2005.
[20] J.M. Lopez, J. Shen, An efficient spectral-projection method for the Navier–Stokes equations in cylindrical geometries I. Axisymmetric cases, J. Comput. Phys. 139 (1998) 308–326.
[21] P.K. Notz, O.A. Basaran, Dynamics and breakup of a contracting liquid filament, J. Fluid Mech. 512 (2004) 223–256.
[22] S. Osher, R. Fedkiw, Level Set Methods and Dynamic Implicit Surfaces, Applied Mathematical Sciences, vol. 153, Springer-Verlag, New York, 2003.
[23] Y. Renardy, M. Renardy, PROST: a parabolic reconstruction of surface tension for the volume-of-fluid method, J. Comput. Phys. 183 (2) (2002) 400–421.
[24] N.D. Robinson, P.H. Steen, Observation of singularity formation during the capillary collapse and bubble pinch-off of a sop film bridge, J. Colloid Interface Sci. 241 (2001) 448–458.
[25] R. Schulkes, The evolution and bifurcation of a pendant drop, J. Fluid Mech. 278 (1994) 83–100.
[26] R. Schulkes, The contraction of liquid filaments, J. Fluid Mech. 309 (1996) 277–300.
[27] T. Seta, K. Kono, S. Chen, Lattice Boltzmann method for two-phase flows, Int. J. Modern Phys. B 17 (2003) 169.
[28] J.A. Sethian, Level Set Methods and Fast Marching Methods, 2nd ed.Cambridge Monographs on Applied and Computational Mathematics, vol. 3, Cambridge University Press, Cambridge, 1999.
[29] J. Shen, Efficient spectral-Galerkin method I. Direct solvers for second- and fourth-order equations using Legendre polynomials, SIAM J. Sci. Comput. 15 (1994) 1489–1505.
[30] J. Shen, Efficient spectral-Galerkin method III. Polar and cylindrical geometries, SIAM J. Sci. Comput. 18 (1997) 1039–1065.
[31] M.R. Swift, W.R. Osborn, J.M. Yeomans, Lattice Boltzmann simulation of nonideal fluids, Phys. Rev. Lett. 75 (1995) 83033.
[32] E.D. Wilkes, S.D. Phillips, O.A. Basaran, Computational and experimental analysis of dynamics of drop formulation, Phys. Fluids 11 (1999) 3577–3598.
[33] P. Yue, J.J. Feng, C. Liu, J. Shen, A diffuse-interface method for simulating two-phase flows of complex fluids, J. Fluid Mech. 515 (1) (2004) 293–317.
[34] P. Yue, J.J. Feng, C. Liu, J. Shen, Diffuse-interface simulations of drop coalescence and retraction in viscoelastic fluids, J. Non-Newtonian Fluid Mech. 129 (2005) 163–176.
[35] P. Yue, J.J. Feng, C. Liu, J. Shen, Interfacial force and Marangoni flow on a nematic drop retracting in an isotropic fluid, J. Colloid Interface Sci. 290 (2005) 281–288.
[36] Raoyang Zhang, Xiaoyi He, Shiyi Chen, Interface and surface tension in incompressible lattice Boltzmann multiphase model, Comput. Phys. Commun. 129 (1–3) (2000) 121–130, Discrete simulation of fluid dynamics (Tokyo, 1999).
[37] X. Zhang, Dynamics of growth and breakup of viscous pendant drops into air, J. Collid Interface Sci. 212 (1999) 107–122.
[38] X. Zhang, O.A. Basaran, An experimental study of dynamics of drop formation, Phys. Fluids 7 (1995) 1184–1203.